J Membrane Biol (2013) 246:355–364
DOI 10.1007/s00232-013-9539-6

ORIGINAL ARTICLES

Mechanistic Basis for Type 2 Long QT Syndrome Caused by *KCNH2* Mutations that Disrupt Conserved Arginine Residues in the Voltage Sensor

Christie M. McBride · Ashley M. Smith · Jennifer L. Smith · Allison R. Reloj · Ellyn J. Velasco · Jonathan Powell · Claude S. Elayi · Daniel C. Bartos · Don E. Burgess · Brian P. Delisle

Received: 17 September 2012 / Accepted: 19 March 2013 / Published online: 2 April 2013

Abstract *KCNH2* encodes the Kv11.1 channel, which conducts the rapidly activating delayed rectifier K^+ current (I_{Kr}) in the heart. *KCNH2* mutations cause type 2 long QT syndrome (LQT2), which increases the risk for life-threatening ventricular arrhythmias. LQT2 mutations are predicted to prolong the cardiac action potential (AP) by reducing I_{Kr} during repolarization. Kv11.1 contains several conserved basic amino acids in the fourth transmembrane segment (S4) of the voltage sensor that are important for normal channel trafficking and gating. This study sought to determine the mechanism(s) by which LQT2 mutations at conserved arginine residues in S4 (R531Q, R531W or R534L) alter Kv11.1 function. Western blot analyses of HEK293 cells transiently expressing R531Q, R531W or R534L suggested that only R534L inhibited Kv11.1 trafficking. Voltage-clamping experiments showed that R531Q or R531W dramatically altered Kv11.1 current ($I_{Kv11.1}$) activation, inactivation, recovery from inactivation and deactivation. Coexpression of wild type (to mimic the patients' genotypes) mostly corrected the changes in $I_{Kv11.1}$ activation and inactivation, but deactivation kinetics were still faster. Computational simulations using a human ventricular AP model showed that accelerating deactivation rates was sufficient to prolong the AP, but these effects were minimal compared to simply reducing I_{Kr}. These are the first data to demonstrate that coexpressing wild type can correct activation and inactivation dysfunction caused by mutations at a critical voltage-sensing residue in Kv11.1. We conclude that some Kv11.1 mutations might accelerate deactivation to cause LQT2 but that the ventricular AP duration is much more sensitive to mutations that decrease I_{Kr}. This likely explains why most LQT2 mutations are nonsense or trafficking-deficient.

Keywords Long QT syndrome · Potassium ion channel · Arrhythmia · Channel gating · Trafficking

C. M. McBride · A. M. Smith · J. L. Smith · A. R. Reloj · E. J. Velasco · J. Powell · D. C. Bartos · D. E. Burgess · B. P. Delisle (✉)
Department of Physiology, Center for Muscle Biology, University of Kentucky, 800 Rose St. MS508, Lexington, KY 40536, USA
e-mail: brian.delisle@uky.edu

C. S. Elayi
Division of Cardiovascular Medicine, Gill Heart Institute, University of Kentucky, Lexington, KY 40536, USA

Introduction

KCNH2 encodes the Kv11.1 voltage-gated K^+ channel α-subunit that underlies the rapidly activating delayed rectifier K^+ current (I_{Kr}) in the heart (Sanguinetti et al. 1995; Trudeau et al. 1995). Mutations in *KCNH2* cause type 2 long QT syndrome (LQT2), an inherited disorder of cardiac excitability (Curran et al. 1995; Sanguinetti et al. 1995). LQT2 mutations cause a loss-of-function in I_{Kr} to prolong ventricular action potential (AP) duration and increase the risk for life-threatening ventricular arrhythmias (Delisle et al. 2004; Sanguinetti et al. 1996; Sanguinetti and Tristani-Firouzi 2006).

Loss-of-function LQT2 mutations can decrease I_{Kr} by reducing channel number at the cell surface membrane, decreasing single-channel conductance and/or altering the open probability. Most commonly, LQT2 is caused by mutations that decrease channel number at the cell surface membrane. About 40 % of LQT2 mutations are radical mutations (nonsense, truncations, splice site or deletion) that decrease Kv11.1 synthesis, and the remaining 60 %

are missense mutations that alter a single amino acid residue (Kapa et al. 2009). LQT2 missense mutations were originally thought to cause long QT syndrome by primarily affecting Kv11.1 deactivation gating; however, more recent studies using mammalian expression systems show that up to 90 % of LQT2 missense mutations decrease the intracellular transport (trafficking) of Kv11.1 to the cell surface membrane (Anderson et al. 2006; Chen et al. 1999; Furutani et al. 1999; Nakajima et al. 1998, 1999; Sanguinetti et al. 1996; Zhou et al. 1998a, 1999).

Kv11.1 contains six transmembrane segments (S1–S6), where S1–S4 form the voltage sensor and S5–S6 comprise the pore domain. S4 contains several highly conserved arginine residues that are important for normal Kv11.1 gating (Papazian et al. 1991; Schulteis et al. 1998; Tiwari-Woodruff et al. 2000). R531 plays a pivotal role in Kv11.1 gating because it is responsible for the normal transfer of Kv11.1 gating charge and it couples with all of the conserved acidic residues in the voltage-sensor domain. Studies show that engineered amino acid substitutions at arginine R531 alter Kv11.1 current ($I_{Kv11.1}$) activation, inactivation and deactivation (Piper et al. 2005, 2008; Subbiah et al. 2004, 2005; Zhang et al. 2004, 2005). Thus far, two LQT2 mutations that alter R531 (R531Q and R531W) and another conserved arginine at R534 (R534L and R534C) have been identified (Kapa et al. 2009; Nakajima et al. 1999; Napolitano et al. 2005; Splawski et al. 2000). The purpose of this study was to determine whether these mutations negatively affect the gating of wild-type Kv11.1 (WT) to cause LQT2.

Materials and Methods

Mutagenesis, Tissue Culture and Transfection

The appropriate nucleotide changes of the LQT2 mutations R531Q, R531W and R534L were engineered in WT cDNA cloned in the pcDNA3 vector using the QuickChange Site Directed Mutagenesis Kit (Agilent Technologies, Santa Clara, CA). The integrity of all the constructs was verified by DNA sequencing (AGTC, University of Kentucky, Lexington, KY). Human embryonic kidney 293 (HEK293) cells were cultured at 37 °C (5 % CO_2) in MEM supplemented with 10 % fetal bovine serum (Invitrogen, Carlsbad, CA). Cells were transfected using Superfect (Qiagen, Valencia, CA) with WT, R531Q, R531W or R534L plasmid DNA (3 μg). For coexpression studies, cells were transfected with equal amounts of WT and mutant Kv11.1 plasmid DNA (1.5 μg each). For electrophysiological studies, cells were also transfected with enhanced green fluorescent protein (GFP) cDNA subcloned in pKR5 (0.3 μg). GFP-positive cells were analyzed using Western blot or the whole-cell patch-clamp technique 48–72 h after transfection.

Western Blot

Cells for Western blotting were harvested with lysis buffer as previously described (Zhou et al. 1998a). Equal amounts of total protein were electrophoresed on a 6.5–7.5 % SDS-polyacrylamide gel, transferred electrophoretically to nitrocellulose and probed with the anti-Kv11.1 (Santa Cruz Biotechnologies, Santa Cruz, CA) and anti-Na^+/K^+-ATPase (Abcam, Cambridge, MA). Protein concentration was measured using the Bio-Rad DC Protein Assay (Bio-Rad, Hercules, CA). For each experiment, protein standards were generated from 2 mg/ml albumin stock by serially diluting BSA stock in 1 % NP-40 buffer. A standard concentration–absorbance curve was generated, and we calculated the lysate sample concentrations from the resulting linear regression. The immunoblots were also probed with a control (anti-Na^+/K^+-ATPase) for the loading and transfer of the protein, which allows for a better comparison between lanes when the loading and transfer might not be uniform (see Fig. 2b, lane 2). Anti-Kv11.1 and anti-Na^+/K^+-ATPase were detected using Odyssey goat anti-rabbit (LI-COR Biosciences, Lincoln, NE) and Odyssey donkey anti-mouse (LI-COR Biosciences), respectively. The LI-COR Odyssey infrared imaging system was used to image and quantify the immunolabeling.

Electrophysiology

Functional analyses were done using a standard whole-cell patch-clamp technique on GFP-positive cells similar to that previously described (Anson et al. 2004; Zhou et al. 1998b). The external solution contained (in mM) 137 NaCl, 4 KCl, 1.8 $CaCl_2$, 1 $MgCl_2$, 10 glucose and 10 HEPES (pH 7.4 with NaOH). An internal pipette solution contained (in mM) 130 KCl, 1 $MgCl_2$, 5 EGTA, 5 MgATP and 10 HEPES (pH 7.2 with KOH). An Axopatch-200B patch-clamp amplifier (Axon Instruments, Union City, CA) was used to measure membrane currents and cell capacitance. The pipette resistances were 1–2 MΩ, and series resistance was compensated up to 95 %. pCLAMP 10 software (Axon Instruments) was used to generate the voltage protocols, to acquire current signals and for data analyses. Origin 7.0 (Microcal, Northhampton, MA) was used for performing Boltzmann curve fitting to the current–voltage (*I–V*) relations and for generating graphs. The data were fit with the Boltzmann equation

$$I = (I_{MIN} - I_{MAX})/\left[\left(1 + e^{(V-V1/2)/k}\right) + I_{MAX}\right]$$

where I_{MIN} is the minimally activated current, I_{MAX} is the maximally activated current, $V½$ is the midpoint potential

for half-maximal activation and k is the slope factor. The holding potential was −80 mV, and the dashed line in the figures indicates zero current.

Computational Modeling

The O'Hara–Virág–Varró–Rudy (OVVR) computational model for an undiseased human cardiac ventricular AP was used to simulate the effect that accelerating I_{Kr} deactivation kinetics has on the time to 90 % ventricular AP repolarization (APD90) (O'Hara et al. 2011). We also compared this to decreasing the relative amplitude of I_{Kr} to mimic trafficking/permeation or synthesis defects.

Statistics

Data are reported as the mean ± standard error (SE). A one-way ANOVA was used to determine if there was difference among the groups, and post hoc analyses using the Dunnett's test were performed to see which group(s) differed compared to WT. Significance was determined at the $p < 0.05$ level.

Results

Kv11.1 contains several highly conserved basic residues that are regularly spaced on the S4 and important for normal gating (Fig. 1) (Piper et al. 2005; Subbiah et al. 2004; Zhang et al. 2004). At least four different LQT2 missense mutations that alter two of these basic residues have been identified (R531Q, R531W, R534L and R534C) (Kapa et al. 2009; Nakajima et al. 1999; Napolitano et al. 2005; Splawski et al. 2000). R531Q, R531W and R534C have been shown to alter Kv11.1 gating when expressed as homomeric channels in *Xenopus* oocytes; however, subsequent studies showed that R534C does not traffic in mammalian cells cultured at physiological temperatures (Anderson et al. 2006; Nakajima et al. 1999; Rossenbacker et al. 2005; Subbiah et al. 2004). We tested whether R531Q, R531W or R534L traffic in HEK293 cells cultured at 37 °C. Kv11.1 is cotranslationally modified in the endoplasmic reticulum (ER) at N598 by the attachment of *N*-linked core glycans to generate a 135-kDa immature glycoprotein, and the glycan moiety undergoes further posttranslational glycosylation in the Golgi apparatus to generate the terminally glycosylated 155-kDa mature Kv11.1 α-subunit (Zhou et al. 1998b). Trafficking-deficient LQT2 mutations can be identified using Western blot analyses because they decrease the relative amount of 155-kDa mature Kv11.1 (mature Kv11.1/total Kv11.1) (Smith et al. 2011; Walker et al. 2010; Zhou et al. 1998a). Based on Western blot analyses, R531Q and R531W appeared to traffic normally, whereas R534L did not (Fig. 2a, b); and coexpressing WT to mimic the patients' genotypes did not facilitate or rescue R534L terminal glycosylation (Fig. 2a). These data suggest that R534L negatively affected the trafficking of WT.

Using the whole-cell patch-clamp technique, we next determined the effect that R531Q, R531W or R534L had on $I_{Kv11.1}$ by applying step-like pulses from −80 to 50 or 100 mV in 10-mV increments for 5 s, followed by a "tail" pulse to −50 mV for 5 s (Fig. 2c). The peak $I_{Kv11.1}$ measured during the tail pulse was plotted as a function of the step-pulse potential, and the data were fit with a Boltzmann function to calculate the mean I_{MAX}, $V½$ and k (Fig. 2d). Compared to cells expressing WT, cells expressing R531Q or R531W dramatically shifted the $V½$ more positive and increased k (Table 1). Cells expressing R534L showed a large reduction in I_{MAX} and a negative shift in $V½$ (Table 1). Surprisingly, coexpressing WT mostly corrected the changes in $I_{Kv11.1}$ gating. Only k was still increased in cells coexpressing WT and R531W (Table 1). We conclude that R531Q and R531W minimally alter $I_{Kv11.1}$ activation in cells coexpressing WT.

The biochemical and functional phenotype of R534L is consistent with it being a trafficking-deficient LQT2 mutation (Anderson et al. 2006; Ficker et al. 2002; Zhou et al. 1998a, 1999). Culturing cells in the class III antiarrhythmic E-4031 increases the trafficking and functional expression for most trafficking-deficient LQT2 mutations (Anderson et al. 2006; Ficker et al. 2002; Zhou et al. 1999). E-4031 is postulated to act as a "pharmacological chaperone" by binding in the Kv11.1 pore (Ficker et al. 2002; Loo and Clarke 1997; Zhou et al. 1999). Pharmacological correction of trafficking-deficient LQT2 mutations can be

```
                        *  *
Kv11.1   GLLKTARLLRLVRVA 536
Kv1.1    RVIRLVRVFRIFKLS 306
Kv2.1    QIFRIMRILRILKLA 311
Kv3.1    RVVRFVRILRIFKLT 325
Kv4.1    VTLRVFRVFRIFKFS 306
Kv5.1    QALRIMRIARIFKLA 304
Kv6.1    RVLRALRILYVMRLA 357
Kv7.1    RGIRFLQILRMLHVD 242
Kv8.1    QVLRLLRALRMLKLG 327
Kv9.1    QVFRLMRIFRVLKLA 356
```

Fig. 1 LQT2 mutations at R531 or R534 disrupt conserved arginine residues in the Kv11.1 S4. Amino acid residue sequence alignments for the S4 of Kv11.1 (NP_000229.1), Kv1.1 (NP_000208.2), Kv2.1 (NP_004966), Kv3.1 (NP_001106212), Kv4.1 (NP_004970), Kv5.1 (NP_002227), Kv6.1 (NP_002228), Kv7.1 (NP_000209), Kv8.1 (NP_055194.1) and Kv9.1 (NP_002242.2). The highly conserved basic amino acid residues are shaded gray

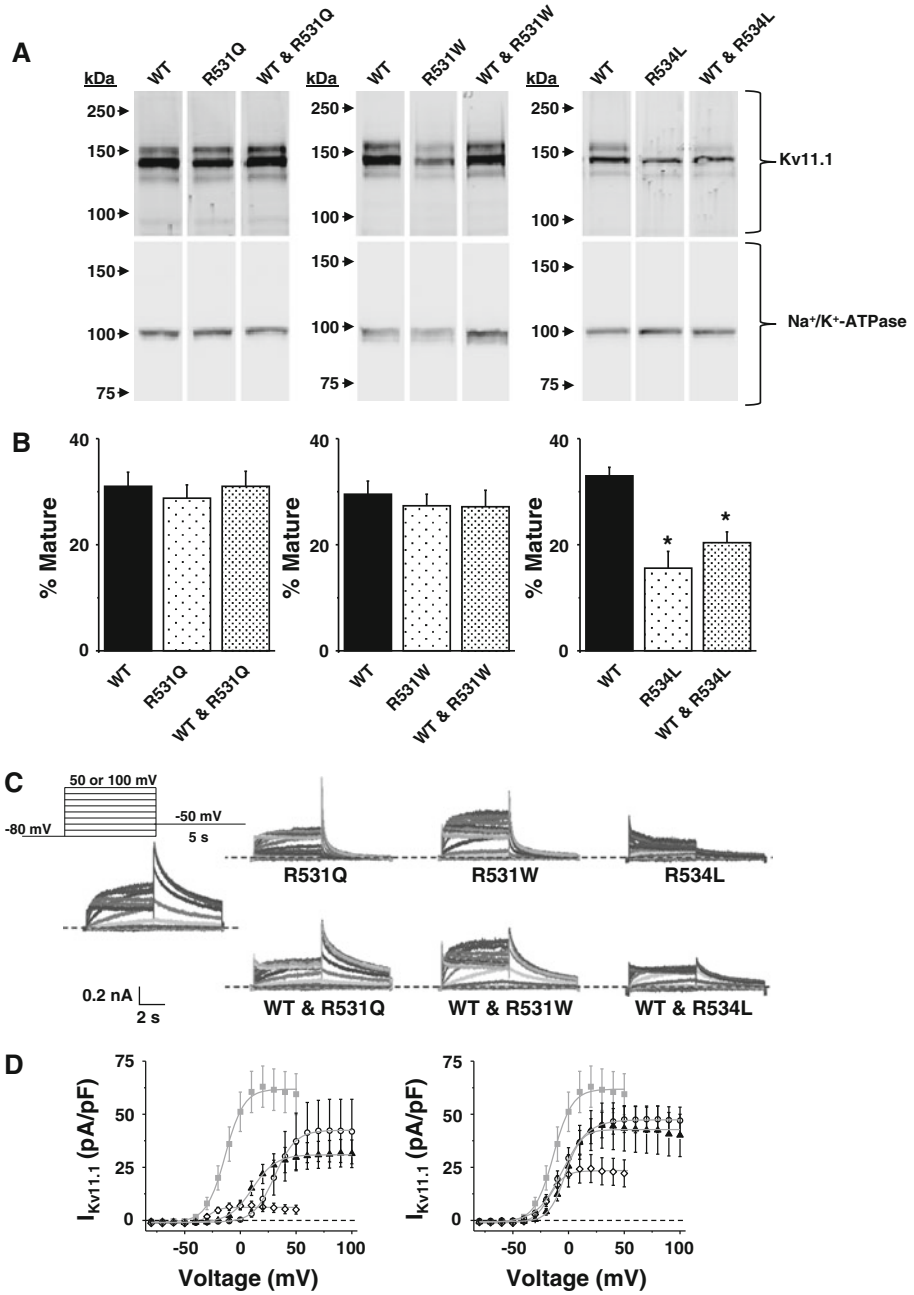

Fig. 2 R531Q and R531W primarily alter $I_{Kv11.1}$ gating. **a** Representative immunoblot analysis of lysates isolated from cells expressing WT, R531Q or WT and R531Q (*left*); WT, R531W or WT and R531W (*middle*); and WT, R534L or WT and R534L (*right*). The immunoblots were probed with anti-Kv11.1 and anti-Na^+/K^+-ATPase as a loading/transfer control. All images are from the same immunoblot and were cropped for presentation purposes. **b** The percent of mature Kv11.1 (mature/total Kv11.1) based on immunoblot analyses for each set of experiments is plotted ($n = 4$–5, $^*p < 0.05$). Each set of probed samples is from the same blot, and the intensity and brightness of the images were not altered. **c** Representative families of currents measured from cells transiently expressing WT, R531Q, R531W, R534L, WT and R531Q, WT and R531W or WT and R534L using the voltage protocol shown. **d***LeftI–V* relations show the mean peak $I_{Kv11.1}$ measured during the tail pulse plotted as a function of the step pulse from cells expressing WT (*gray squares*), R531Q (*open circles*), R531W (*black triangles*) or R534L (*open diamonds*). *RightI–V* relations show the mean peak $I_{Kv11.1}$ measured during the tail pulse plotted as a function of the step-pulse potential from cells expressing WT (*gray squares*), WT and R531Q (*open circles*), WT and R531W (*black triangles*) or WT and R534L (*open diamonds*). Individual data were fit using a Boltzmann equation (*solid line*) to calculate the mean I_{MAX}, $V½$ and k (Table 1)

visualized using Western blot analyses because it increases the relative amount of mature Kv11.1. Using Western blot analyses, we found that culturing cells expressing R534L in E-4031 increased the relative amount of mature Kv11.1 (Fig. 3a, b). Moreover, we found that culturing cells in E-4031 increased $I_{Kv11.1}$ after drug washout (Fig. 3c, d).

Table 1 Mean parameters calculated from the Boltzmann fits to $I_{Kv11.1}$ measured from cells expressing WT, R531Q, R531W, R534L, WT and R531Q, WT and R531W, WT and R534L

Expressed	I_{MAX}	$V½$	k	n
WT	62 ± 10	–14 ± 3	6.2 ± 0.2	19
R531Q	42 ± 15	32 ± 2*	9.4 ± 1*	9
R531W	33 ± 6	12 ± 2*	9.8 ± 0.7*	13
R534L	7 ± 2*	–28 ± 1	4.6 ± 0.4	11
WT and R531Q	48 ± 6	–3 ± 3	10.2 ± 0.6*	18
WT and R531W	43 ± 11	–4 ± 2	7.2 ± 0.7	12
WT and R534L	23 ± 6*	–18 ± 2	6.3 ± 0.3	10

*$p < 0.05$ compared to WT

These data suggest that R534L is a trafficking-deficient LQT2 mutation that undergoes pharmacological correction with E-4031.

Since R534L appeared to primarily reduce $I_{Kv11.1}$ by inhibiting trafficking, we focused the rest of our analyses on R531Q and R531W. We next determined whether R531Q or R531W altered $I_{Kv11.1}$ inactivation. We measured the development of inactivation by depolarizing cells to 50 mV for 1.5 s, hyperpolarizing to −100 mV for 10 ms to reopen most channels and then applying a test pulse from 0 to 90 mV in 10-mV increments for 3 s (Fig. 4a). The $I_{Kv11.1}$ decay measured during the test pulse was described as a single-exponential process and used to calculate a time constant for the development of $I_{Kv11.1}$ inactivation (τ_{inact}) (Fig. 4b). Compared to cells expressing WT, cells expressing R531Q or R531W showed a positive or depolarizing shift in τ_{inact}. Coexpressing WT partially corrected this for R531W but not R531Q. The rate for the recovery of $I_{Kv11.1}$ inactivation was also measured by prepulsing cells to 50 mV for 5 s, followed by a test pulse from −120 to −30 mV for 1.5 s (Fig. 4c). To calculate the time constant for recovery from $I_{Kv11.1}$ inactivation (τ_{rec}), the rising phase of $I_{Kv11.1}$ measured during the test pulse was described as a single-exponential process, and these rates were plotted as a function of the test-pulse potential (Fig. 4d). Cells expressing R531Q or R531W accelerated recovery of Kv11.1 inactivation kinetics by causing a positive shift in the voltage dependence for τ_{rec}; however, coexpression of WT with either R531Q or R531W almost completely corrected this. We conclude that R531Q and R531W slightly slow the development of $I_{Kv11.1}$ inactivation in cells coexpressing WT.

Acceleration of Kv11.1 deactivation kinetics has been implicated as a cause for LQT2 (Berecki et al. 2005; Chen et al. 1999). To test if R531Q or R531W accelerated $I_{Kv11.1}$ deactivation, $I_{Kv11.1}$ deactivation rates were measured from cells by applying a 2-s prepulse to 50 mV, followed by a test pulse from −120 to −30 mV for 10 s in 10-mV increments (Fig. 5a). Deactivation rates were calculated by

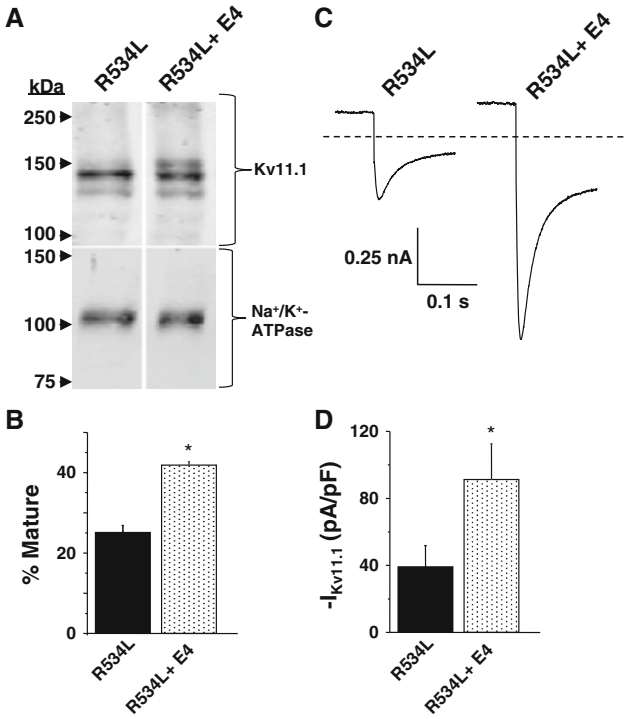

Fig. 3 R534L is a trafficking-deficient LQT2 mutation that undergoes pharmacological correction with E-4031. **a** Representative immunoblot analysis of lysates isolated from cells expressing R534L in control conditions or cultured in E-4031 (E4) (10 μM for 48 h). Immunoblots were probed with anti-Kv11.1 and anti-Na^+/K^+-ATPase as a loading/transfer control. All images are from the same immunoblot and were cropped for presentation purposes. **b** The percent of mature Kv11.1 (mature/total Kv11.1) based on immunoblot analyses is plotted ($n = 4$, *$p < 0.05$). **c** Representative current traces measured from cells transiently expressing R534L in control conditions or cultured with E-4031. Cells were depolarized to 50 mV for 3 s so as to maximally activate R534L and then hyperpolarized to −120 mV for 3 s. Traces show the inward current that was measured at the very beginning of the tail pulse to −120 mV. **d** The corresponding mean peak tail current is plotted ($n = 7$–10 cells, *$p < 0.05$)

describing the decay of $I_{Kv11.1}$ measured during the test pulse as a double-exponential process with a fast and a slow time component (τ_{fast} and τ_{slow}), and the time constants were plotted as a function of the test-pulse potential (Figs. 5b, 5c). Additionally, the relative percent amplitude of the slow component was plotted as a function of the test-pulse potential (Fig. 5d). Compared to cells expressing WT, cells expressing R531Q and R531W showed ~10-fold faster τ_{fast} and τ_{slow} for many of the test-pulse potentials. Coexpressing WT and R531Q or R531W only partially corrected the faster deactivation rates, but τ_{fast} and τ_{slow} were still severalfold faster at most test-pulse potentials >−80 mV. Compared to WT, the relative amplitude of the slow component was voltage-independent in cells expressing R531Q or R531W; however, this was completely corrected by coexpression of WT.

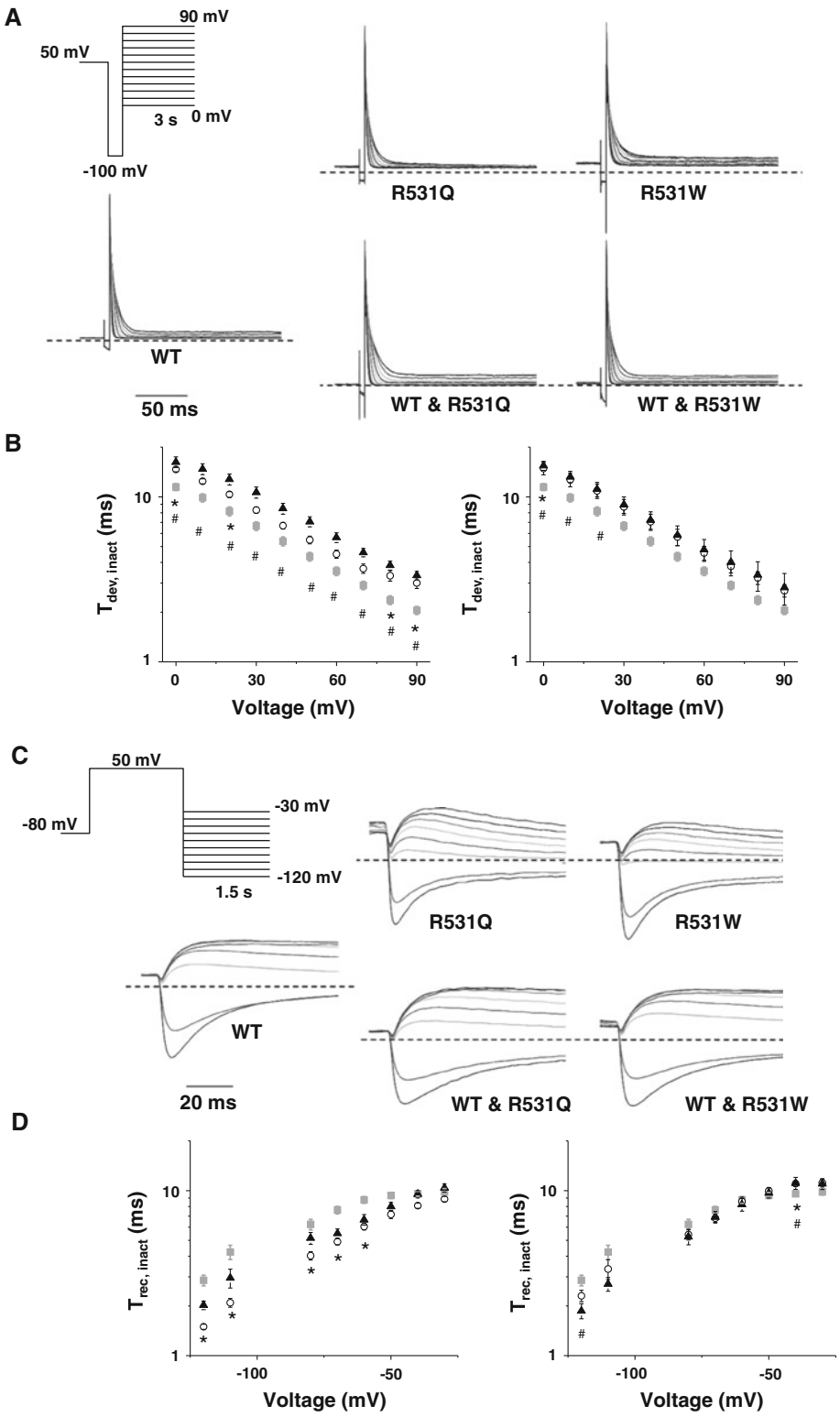

Fig. 4 R531Q and R531W slow the development of inactivation. **a** Representative families of currents measured from cells transiently expressing WT, R531Q, R531W, WT and R531Q or WT and R531W using the voltage protocol shown. The τ_{inact} was calculated by describing the decay of $I_{Kv11.1}$ measured during the test pulse as a single exponential. **b** *Left* Mean τ_{inact} calculated from cells expressing WT (*gray squares*), R531Q (*open circles*) or R531W (*black triangles*) plotted as a function of the test pulse. *Right* Mean τ_{inact} calculated from cells expressing WT (*gray squares*), WT and R531Q (*open circles*) or WT and R531W (*black triangles*) plotted as a function of the test pulse ($n \geq 7$). **c** Representative families of currents measured from cells expressing WT, R531Q, R531W, WT and R531Q or WT and R531W using the voltage protocol shown. The τ_{rec} was calculated by describing the rising phase of $I_{Kv11.1}$ measured during the test pulse as a single exponential. **d** *Left* Mean τ_{rec} calculated from cells expressing WT (*gray squares*), R531Q (*open circles*) or R531W (*black triangles*) plotted as a function of the test pulse. *Right* Mean τ_{inact} calculated from cells expressing WT (*gray squares*), WT and R531Q (*open circles*) or WT and R531W (*black triangles*) plotted as a function of the test pulse ($n \geq 7$). Compared to WT, $p < 0.05$ for R531Q (*asterisks*) or R531W (*hash*)

R531Q and R531W mainly affect $I_{Kv11.1}$ in cells coexpressing WT by slowing inactivation and accelerating deactivation kinetics. Slower inactivation kinetics is not expected to cause a loss of I_{Kr} function, but faster deactivation kinetics have been associated with the LQT2 mutations R56Q and ΔY475 (Berecki et al. 2005; Chen et al. 1999; Lin et al. 2010; Nakajima et al. 1999). We tested the impact that accelerating I_{Kr} deactivation kinetics 10-fold has on the ventricular APD90 using the OVVR computational model of a human AP pulsed at 1 Hz.

Figure 6a shows the ventricular AP waveforms and the corresponding I_{Kr} for a control simulation or a simulation with 10-fold accelerated I_{Kr} deactivation kinetics. The faster deactivation kinetics prolonged the ventricular APD90 waveform by $\sim$10 %. In the control simulation, I_{Kr} is present during the upstroke and persists for the entire duration of the AP waveform. Simulations incorporating faster deactivation kinetics caused a loss of I_{Kr} during the initial upstroke, and it did not persist throughout the AP waveform (Fig. 6a). This suggests that I_{Kr} with faster deactivation kinetics completely deactivates during the repolarization and diastolic phase.

The vast majority of LQT2 nonsense mutations and missense mutations are expected to simply decrease I_{Kr} by inhibiting the number of channels at the cell surface membrane. Indeed, only two other LQT2 mutations, R56Q and ΔY475, are expected to cause LQT2 by accelerating deactivation kinetics. We compared the effect that either faster deactivation kinetics or decreasing I_{Kr} had on the APD90 (Fig. 6b). The modeling suggested that $\sim$100-fold acceleration in I_{Kr} deactivation kinetics was needed to mimic haploinsufficiency ($\sim$50 % reduction in I_{Kr}). In other words, the APD90 is much more sensitive to changes in the amplitude of I_{Kr} than deactivation kinetics. This

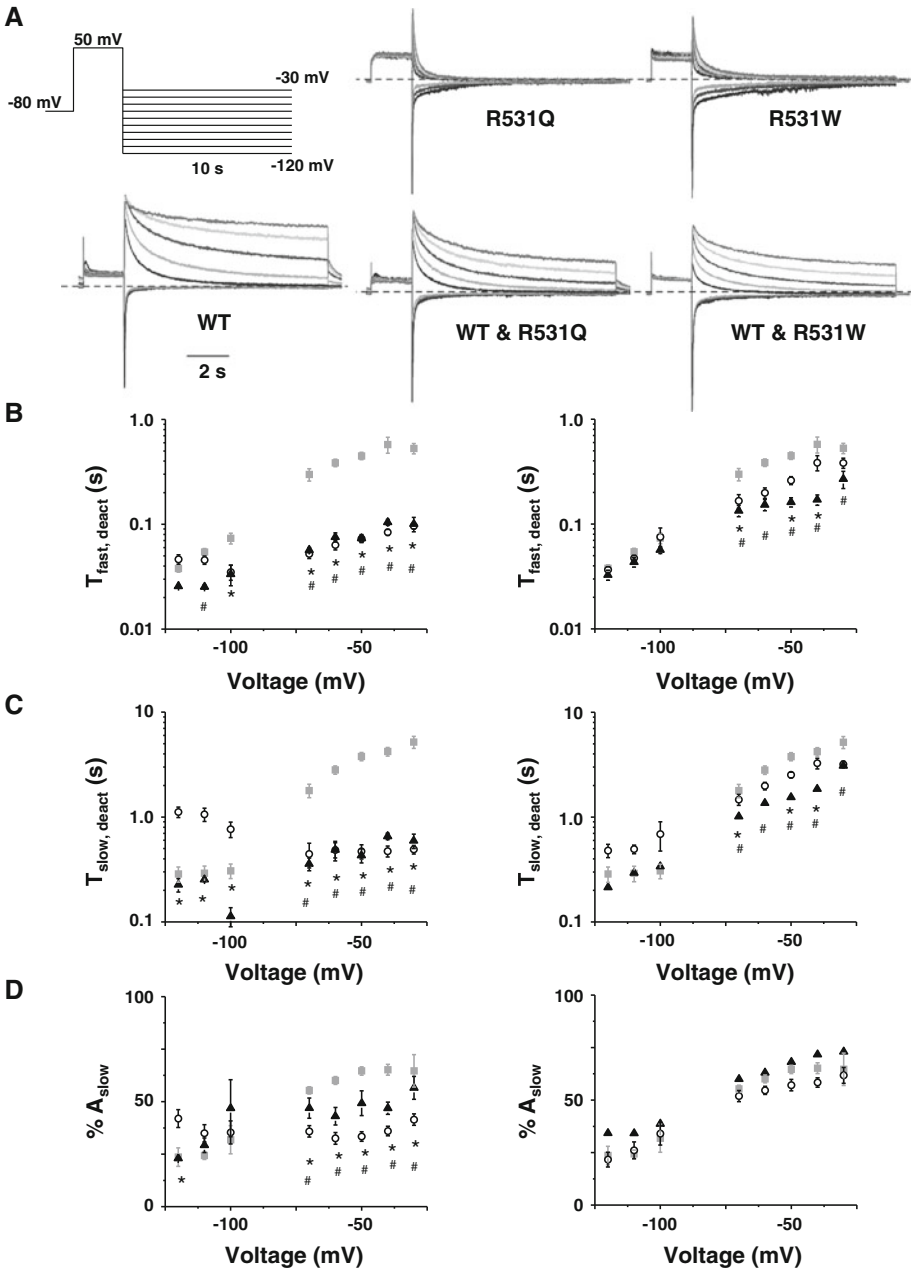

Fig. 5 R531Q and R531W speed $I_{Kv11.1}$ deactivation. **a** Representative families of currents measured from cells expressing WT, R531Q, R531W, WT and R531Q or WT and R531W using the voltage protocol shown. **b**–**d** *Left* Mean τ_{fast} (**b**) and τ_{slow} (**c**) and percent amplitude of the current that deactivated with the slow component (*% Amp$_{slow}$*, **d**) plotted as a function of the test pulse measured from cells expressing WT (*gray squares*), R531Q (*open circles*) or R531W (*black triangles*). *Right* Mean τ_{fast} (**b**) and τ_{slow} (**c**) and % Amp$_{slow}$ (**d**) plotted as a function of the test pulse measured from cells expressing WT (*gray squares*), WT and R531Q (*open circles*) or WT and R531W (*black triangles*). Compared to WT, $p < 0.05$ for R531Q (*asterisks*) or R531W (*hash*)

likely explains why most causative LQT2 missense mutations are predicted to decrease the trafficking of Kv11.1 rather than accelerate deactivation kinetics (Fig. 6c) (Anderson et al. 2006; Ficker et al. 2002; Furutani et al. 1999; Gianulis and Trudeau 2011; Guo et al. 2012; Harley et al. 2012; Rossenbacker et al. 2005; Zhou et al. 1998a, 1999).

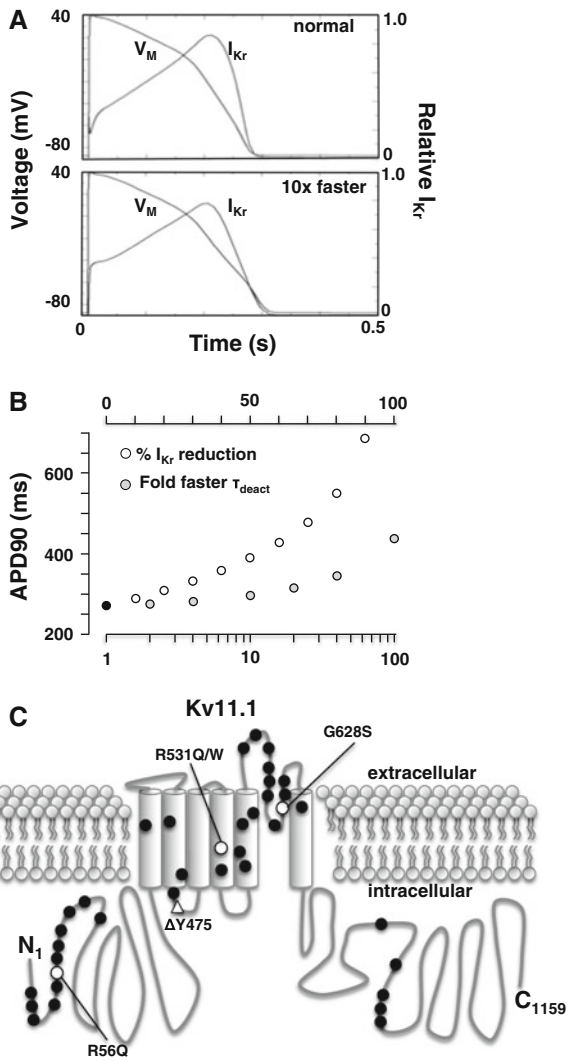

Fig. 6 Accelerated deactivation kinetics predicts a prolongation in the ventricular APD90. **a** Shown are the steady-state ventricular AP waveforms (V_M) and the corresponding I_{Kr} for a control simulation (*normal*) or one with the deactivation kinetics accelerated 10-fold (10× faster) pulsed at 1 Hz. **b** Shown are the APD90 for a control simulation (*black circle*), simulations that reduce I_{Kr} (*open circles*) and simulations that accelerate deactivation (*gray circles*) by the indicated factor. The cycle length for the simulations was 1 Hz. **c** An individual Kv11.1 α-subunit with an intracellular amino terminal (N_1), six transmembrane segments and the carboxy terminal (C_{1159}). The relative locations of LQT2 missense (*circles*) or deletion (*triangle*) mutations expressed in HEK293 cells are shown. LQT2 mutations that primarily disrupt trafficking in mammalian cells are shown in *black*. LQT2 mutations that traffic are shown in *white*. R56Q, ΔY475, R531Q and R531W accelerate deactivation rates; and G628S likely disrupts K^+ permeation by altering the selectivity filter

Discussion

The purpose of this study was to understand the mechanism(s) by which LQT2 mutations that disrupt conserved arginine residues in the S4 cause LQT syndrome. Our data suggest that homomeric R531Q and R531W channels dramatically altered Kv11.1 gating but that R534L decreased $I_{Kv11.1}$ by reducing Kv11.1 trafficking. Although homomeric R531Q and R531W channels showed dramatic changes in $I_{Kv11.1}$ activation, inactivation and deactivation, coexpression of WT normalized most of these changes. However, accelerated $I_{Kv11.1}$ deactivation kinetics were still observed in cells coexpressing WT and R531Q or R531W, and our computational modeling suggested that this functional phenotype was sufficient to prolong the ventricular AP. Nevertheless, it should be noted that the AP duration was much more sensitive in decreasing I_{Kr} rather than accelerating deactivation kinetics. This latter finding likely explains why a vast majority of LQT2 radical and missense mutations decrease the number of functional channels in the cell surface membrane.

Interestingly, coexpression of WT seems to largely correct profound gating changes caused by several different LQT2 mutations. Similar effects are seen with the LQT2 mutations that localize to the N-terminal Per-Arnt-Sim (NPAS) domain. For example, Rossenbacker and colleagues (2005) showed that cells expressing the LQT2 mutation K28E alone decreased Kv11.1 trafficking and accelerated deactivation rates but that cells coexpressing WT and K28E showed only decreased trafficking (and normal deactivation rates). Similar results are seen with other LQT2 mutations in the NPAS domain (Chen et al. 1999). The NPAS domain interacts with S4–S5 to slow Kv11.1 deactivation gating, and studies suggest that LQT2 mutations in the NPAS domain accelerate $I_{Kv11.1}$ deactivation by disrupting this interaction. Indeed, recent studies show that simply coexpressing the WT NPAS domain alone was sufficient to correct the dysfunctional deactivation gating caused by NPAS LQT2 mutations. We suspect that coexpression of WT and NPAS LQT2 mutations might generate heteromeric channels where the NPAS domain of the WT subunit can substitute for the mutant NPAS domain of the LQT2 subunit to normalize deactivation. Our data now show that coexpression of WT can also correct the activation, inactivation and, to a certain extent, deactivation dysfunction caused by R531 mutations. This was unexpected because R531 is a critical residue involved in Kv11.1 voltage sensing and its effects on homomeric channels is very pronounced. We suggest that the gating of

Kv11.1 channels is largely cooperative and that the presence of WT subunits can also mostly correct the gating dysfunction caused by LQT2 mutations outside the NPAS domain.

There are several limitations to this study. The number of LQT2 patients with these mutations is limited, and additional family-specific factors may contribute to their clinical phenotypes. These data were obtained in a widely used heterologous overexpression system, and not all of the possible Kv11.1 isoforms were studied. Although we transfected equal amounts of WT and mutant Kv11.1 cDNA, we do not know the exact ratio of the WT and mutant subunits. It is possible that the $I_{Kv11.1}$ in the cotransfection mostly reflected WT channels. However, we suspect this is unlikely since R531Q or R531W readily formed functional channels in cells that do not express WT.

In summary, this study suggests LQT2 mutations that disrupt a critical residue in the voltage sensing of Kv11.1 dramatically alter gating, but this is largely normalized by coexpression of WT. Although these mutations sufficiently speed the deactivation kinetics to predict a prolongation in the ventricular AP, we found that the AP duration was much more sensitive to decreases in I_{Kr}. These data likely help to explain why the vast majority of LQT2 mutations do not appear to cause gating dysfunction but rather decrease the number of functional Kv11.1 channels in the cell surface membrane.

This work was supported by the American Heart Association predoctoral award PRE7370003 (to D. C. B.) and the National Heart Lung and Blood Institute grant R01 HL087039 (to B. P. D.).

References

Anderson CL, Delisle BP, Anson BD, Kilby JA, Will ML, Tester DJ, Gong Q, Zhou Z, Ackerman MJ, January CT (2006) Most LQT2 mutations reduce Kv11.1 (hERG) current by a class 2 (trafficking-deficient) mechanism. Circulation 113:365–373

Anson BD, Ackerman MJ, Tester DJ, Will ML, Delisle BP, Anderson CL, January CT (2004) Molecular and functional characterization of common polymorphisms in HERG (KCNH2) potassium channels. Am J Physiol Heart Circ Physiol 286:H2434–H2441

Berecki G, Zegers JG, Verkerk AO, Bhuiyan ZA, de Jonge B, Veldkamp MW, Wilders R, van Ginneken AC (2005) HERG channel (dys)function revealed by dynamic action potential clamp technique. Biophys J 88:566–578

Chen J, Zou A, Splawski I, Keating MT, Sanguinetti MC (1999) Long QT syndrome–associated mutations in the Per-Arnt-Sim (PAS) domain of HERG potassium channels accelerate channel deactivation. J Biol Chem 274:10113–10118

Curran ME, Splawski I, Timothy KW, Vincent GM, Green ED, Keating MT (1995) A molecular basis for cardiac arrhythmia: HERG mutations cause long QT syndrome. Cell 80:795–803

Delisle BP, Anson BD, Rajamani S, January CT (2004) Biology of cardiac arrhythmias: ion channel protein trafficking. Circ Res 94:1418–1428

Ficker E, Obejero-Paz CA, Zhao S, Brown AM (2002) The binding site for channel blockers that rescue misprocessed human long QT syndrome type 2 ether-a-gogo-related gene (HERG) mutations. J Biol Chem 277:4989–4998

Furutani M, Trudeau MC, Hagiwara N, Seki A, Gong Q, Zhou Z, Imamura S, Nagashima H, Kasanuki H, Takao A, Momma K, January CT, Robertson GA, Matsuoka R (1999) Novel mechanism associated with an inherited cardiac arrhythmia: defective protein trafficking by the mutant HERG (G601S) potassium channel. Circulation 99:2290–2294

Gianulis EC, Trudeau MC (2011) Rescue of aberrant gating by a genetically encoded PAS (Per-Arnt-Sim) domain in several long QT syndrome mutant human ether-a-go–go-related gene potassium channels. J Biol Chem 286:22160–22169

Guo J, Zhang X, Hu Z, Zhuang Z, Zhu Z, Chen Z, Chen W, Zhao Z, Zhang C, Zhang Z (2012) A422T mutation in HERG potassium channel retained in ER is rescurable by pharmacologic or molecular chaperones. Biochem Biophys Res Commun 422: 305–310

Harley CA, Jesus CS, Carvalho R, Brito RM, Morais-Cabral JH (2012) Changes in channel trafficking and protein stability caused by LQT2 mutations in the PAS domain of the HERG channel. PLoS ONE 7:e32654

Kapa S, Tester DJ, Salisbury BA, Harris-Kerr C, Pungliya MS, Alders M, Wilde AA, Ackerman MJ (2009) Genetic testing for long-QT syndrome: distinguishing pathogenic mutations from benign variants. Circulation 120:1752–1760

Lin EC, Holzem KM, Anson BD, Moungey BM, Balijepalli SY, Tester DJ, Ackerman MJ, Delisle BP, Balijepalli RC, January CT (2010) Properties of WT and mutant hERG K^+ channels expressed in neonatal mouse cardiomyocytes. Am J Physiol Heart Circ Physiol 298:H1842–H1849

Loo TW, Clarke DM (1997) Correction of defective protein kinesis of human P-glycoprotein mutants by substrates and modulators. J Biol Chem 272:709–712

Nakajima T, Furukawa T, Tanaka T, Katayama Y, Nagai R, Nakamura Y, Hiraoka M (1998) Novel mechanism of HERG current suppression in LQT2: shift in voltage dependence of HERG inactivation. Circ Res 83:415–422

Nakajima T, Furukawa T, Hirano Y, Tanaka T, Sakurada H, Takahashi T, Nagai R, Itoh T, Katayama Y, Nakamura Y, Hiraoka M (1999) Voltage-shift of the current activation in HERG S4 mutation (R534C) in LQT2. Cardiovasc Res 44: 283–293

Napolitano C, Priori SG, Schwartz PJ, Bloise R, Ronchetti E, Nastoli J, Bottelli G, Cerrone M, Leonardi S (2005) Genetic testing in the long QT syndrome: development and validation of an efficient approach to genotyping in clinical practice. JAMA 294: 2975–2980

O'Hara T, Virag L, Varro A, Rudy Y (2011) Simulation of the undiseased human cardiac ventricular action potential: model formulation and experimental validation. PLoS Comput Biol 7:e1002061

Papazian DM, Timpe LC, Jan YN, Jan LY (1991) Alteration of voltage-dependence of Shaker potassium channel by mutations in the S4 sequence. Nature 349:305–310

Piper DR, Hinz WA, Tallurri CK, Sanguinetti MC, Tristani-Firouzi M (2005) Regional specificity of human ether-à-go–go-related gene channel activation and inactivation gating. J Biol Chem 280: 7206–7217

Piper DR, Rupp J, Sachse FB, Sanguinetti MC, Tristani-Firouzi M (2008) Cooperative interactions between R531 and acidic residues in the voltage sensing module of hERG1 channels. Cell Physiol Biochem 21:37–46

Rossenbacker T, Mubagwa K, Jongbloed RJ, Vereecke J, Devriendt K, Gewillig M, Carmeliet E, Collen D, Heidbuchel H, Carmeliet

P (2005) Novel mutation in the Per-Arnt-Sim domain of KCNH2 causes a malignant form of long-QT syndrome. Circulation 111:961–968

Sanguinetti MC, Jurkiewicz NK (1990) Two components of cardiac delayed rectifier K^+ current. Differential sensitivity to block by class III antiarrhythmic agents. J Gen Physiol 96:195–215

Sanguinetti MC, Tristani-Firouzi M (2006) hERG potassium channels and cardiac arrhythmia. Nature 440:463–469

Sanguinetti MC, Jiang C, Curran ME, Keating MT (1995) A mechanistic link between an inherited and an acquired cardiac arrhythmia: HERG encodes the I_{Kr} potassium channel. Cell 81:299–307

Sanguinetti MC, Curran ME, Spector PS, Keating MT (1996) Spectrum of HERG K^+-channel dysfunction in an inherited cardiac arrhythmia. Proc Natl Acad Sci USA 93:2208–2212

Schulteis CT, Nagaya N, Papazian DM (1998) Subunit folding and assembly steps are interspersed during Shaker potassium channel biogenesis. J Biol Chem 273:26210–26217

Smith JL, McBride CM, Nataraj PS, Bartos DC, January CT, Delisle BP (2011) Trafficking-deficient hERG K channels linked to long QT syndrome are regulated by a microtubule-dependent quality control compartment in the ER. Am J Physiol Cell Physiol 301: C75–C85

Splawski I, Shen J, Timothy KW, Lehmann MH, Priori S, Robinson JL, Moss AJ, Schwartz PJ, Towbin JA, Vincent GM, Keating MT (2000) Spectrum of mutations in long-QT syndrome genes. KVLQT1, HERG, SCN5A, KCNE1, and KCNE2. Circulation 102:1178–1185

Subbiah RN, Clarke CE, Smith DJ, Zhao J, Campbell TJ, Vandenberg JI (2004) Molecular basis of slow activation of the human ether-a-go–go related gene potassium channel. J Physiol 558:417–431

Subbiah RN, Kondo M, Campbell TJ, Vandenberg JI (2005) Tryptophan scanning mutagenesis of the HERG K^+ channel: the S4 domain is loosely packed and likely to be lipid exposed. J Physiol 569:367–379

Tiwari-Woodruff SK, Lin MA, Schulteis CT, Papazian DM (2000) Voltage-dependent structural interactions in the Shaker K^+ channel. J Gen Physiol 115:123–138

Trudeau MC, Warmke JW, Ganetzky B, Robertson GA (1995) HERG, a human inward rectifier in the voltage-gated potassium channel family. Science 269:92–95

Walker VE, Wong MJ, Atanasiu R, Hantouche C, Young JC, Shrier A (2010) Hsp40 chaperones promote degradation of the HERG potassium channel. J Biol Chem 285:3319–3329

Zhang M, Liu J, Tseng GN (2004) Gating charges in the activation and inactivation processes of the HERG channel. J Gen Physiol 124:703–718

Zhang M, Liu J, Jiang M, Wu DM, Sonawane K, Guy HR, Tseng GN (2005) Interactions between charged residues in the transmembrane segments of the voltage-sensing domain in the hERG channel. J Membr Biol 207:169–181

Zhou Z, Gong Q, Epstein ML, January CT (1998a) HERG channel dysfunction in human long QT syndrome. Intracellular transport and functional defects. J Biol Chem 273:21061–21066

Zhou Z, Gong Q, Ye B, Fan Z, Makielski JC, Robertson GA, January CT (1998b) Properties of HERG channels stably expressed in HEK 293 cells studied at physiological temperature. Biophys J 74:230–241

Zhou Z, Gong Q, January CT (1999) Correction of defective protein trafficking of a mutant HERG potassium channel in human long QT syndrome. Pharmacological and temperature effects. J Biol Chem 274:31123–31126